New Journal of Physics
The open-access journal for physics

Analysis of the electronic structure of copper via two-dimensional photoelectron momentum distribution patterns

Aimo Winkelmann[1,3], Christian Tusche[1], A Akin Ünal[1], Martin Ellguth[1], Jürgen Henk[2] and Jürgen Kirschner[1]

[1] Max Planck Institute of Microstructure Physics, Weinberg 2, 06120 Halle, Germany
[2] Martin-Luther-Universität Halle-Wittenberg, Institut für Physik, FG Theoretische Physik, Von-Seckendorff-Platz 1, 06120 Halle, Germany
E-mail: winkelm@mpi-halle.mpg.de

New Journal of Physics **14** (2012) 043009 (18pp)
Received 3 February 2012
Published 11 April 2012
Online at http://www.njp.org/
doi:10.1088/1367-2630/14/4/043009

Abstract. Using a unique *momentum microscope*, we measured energy-resolved momentum distributions of valence-band electrons photoemitted into the whole half-space above the Cu(111) and Cu(001) surfaces. The experimental results are compared to one-step photoemission calculations. Convincing agreement between theoretical and experimental photoelectron momentum patterns can only be achieved by orbital-dependent corrections which emulate many-body self-energy effects in the electronic structure of Cu (Strocov *et al* 2002 *Phys. Rev.* B **66** 195104). By the analysis of the Shockley surface state of Cu(111), we show that these self-energy corrections also affect the surface electronic structure in specific ways. We find that the Shockley surface state of Cu(111) is shifted differently in energy than the bulk states. As a consequence, the agreement between the theoretically calculated and the experimentally measured binding energy of this surface state is improved. Energy-resolved two-dimensional valence-band photoelectron mapping provides an alternative means of determining self-energy values experimentally.

[3] Author to whom any correspondence should be addressed.

Contents

1. Introduction **2**
2. Experiment **3**
3. Theory **3**
4. Results **5**
4.1. Cu(001) 5
4.2. Cu(111) 9
5. Summary **15**
References **16**

1. Introduction

The crystal-momentum-resolved electronic structure is a central concept in solid-state physics. A key aspect that needs to be treated by models of electronic structure is that electrons in a solid form an interacting many-body system and thus cannot strictly be described as independent particles. The premier tool for experimental access to these electronic states is angle-resolved photoelectron spectroscopy (ARPES) [1–5].

Photoelectron spectroscopy measures the energy of removal of one electron from the sample and is thus closely related to the spectral function which contains the excitation energies of the many-body system. Compared to the bare energy of electrons in a non-interacting system, the quasiparticle states of the interacting system are characterized by a shift of the energy and by a finite lifetime. These two effects are described by the real and imaginary parts, respectively, of the energy- and momentum-dependent self-energy (see e.g. [6–9]).

As investigations of important problems in current solid-state research are driven by feedback between experimental ARPES investigations and theoretical calculations, it remains important to test the ability of theoretical models to quantitatively describe photoelectron spectroscopy measurements. For example, as the electrons near the Fermi level are decisive for a considerable number of material properties, the possibility to map the Fermi surface by photoemission represents an especially powerful tool [10–17]. In addition to the crystal-momentum space iso-energy surfaces at the Fermi level, similar measurements in an extended energy range from occupied and unoccupied states provide additional insights into the general effects of interactions on the electronic structure. Moreover, complementary to the reciprocal-space information, much interest is also being focused on the real-space distribution of electronic states [18–20] and the orbital-resolved contributions in the electronic structure of crystals [21, 22] and molecules [23].

In this paper, we present the results of a special experimental approach to valence-band photoemission, with the Cu(001) and Cu(111) surfaces as well-known model systems. The main idea of our experiment is the systematic parallel collection of energy-resolved two-dimensional (2D) angular photoelectron distributions [21, 24–28]. Specifically, we are using an exceptional *momentum microscope* [29] that can detect energy-resolved photoemission intensities in the whole emission hemisphere above the sample surface with extreme efficiency, including optional spin-polarization analysis [30]. The experimental photoelectron momentum patterns in an extended valence-band energy range include the combined effects of bulk states as well as surface states extending in low-symmetry directions over the full surface Brillouin

zone, and thus represent a challenging benchmark for theoretical photoemission models. As we will show, the parallel recording of constant-energy valence-band photoelectron momentum distributions with the momentum microscope allows for a stringent test of theoretical one-step photoemission models because of the sensitivity of the observed momentum-space fine structure to the energy levels of surface and bulk electronic states.

In particular, we will show that sufficiently good agreement between the theoretical and experimental 2D valence-band photoelectron momentum patterns can only be obtained by the application of orbital-dependent corrections for many-body self-energy effects in the electronic structure of copper, which still serves as a standard system for photoemission investigations. The electronic structure of copper has been thoroughly investigated in experiment [31–36] and theory [37–41]. Recently, for the Cu bulk electronic structure, self-energy corrections to the independent-particle density functional theory (DFT) calculations using the local density approximation (LDA) have been established in experimental studies of [35]. These previous results provide estimations of the size of self-energy corrections which we can test in our DFT–LDA one-step photoemission calculations in comparison to the experimental results. Momentum mapping of photoelectrons in the momentum microscope thus provides us with extensive information for potential improvements of theoretical concepts underlying one-step photoemission calculations.

The paper is organized as follows. We introduce the experimental details in section 2, followed by a description of the theoretical model used for the photoemission simulations in section 3. The results are presented in section 4. In section 5, we give a summary of this investigation.

2. Experiment

The momentum microscope used in this investigation is an advanced combination of a photoelectron emission microscope column with an aberration-corrected electrostatic electron energy analyzer [29]. The instrument can detect energy-resolved and (k_x, k_y)-resolved photoemission intensities of photoelectrons emitted into the whole emission hemisphere above the sample surface. The energy resolution was estimated as 170 meV and the momentum resolution as $\pm 0.04\ \text{Å}^{-1}$ by measurements of the Cu(111) Shockley surface state [29].

Clean surfaces of Cu(111) and Cu(001) were prepared by standard procedures. During the measurements, the samples were kept at $-100\ ^{\circ}\text{C}$ by liquid nitrogen cooling.

The coordinate system of the present investigation is shown in figure 1. In this study, we used unpolarized and non-monochromatized HeI radiation, which is incident along the angles $\vartheta = 65^{\circ}$ and $\varphi = 30^{\circ}$, as can be seen from figure 1. The electron-optical axis of the momentum microscope is along the z-direction.

3. Theory

The calculations of both the electronic structure and photoemission intensities rely on the LDA to DFT, using a relativistic multiple-scattering approach (layer-Korringa–Kohn–Rostoker (LKKR)). Solving the Dirac equation, spin–orbit coupling is included. We use the Perdew–Wang exchange-correlation functional [42].

The electronic-structure calculations were performed for semi-infinite systems which comprise the bulk, the surface region and the vacuum. The lattice constant of Cu was $4.83\,a_0$

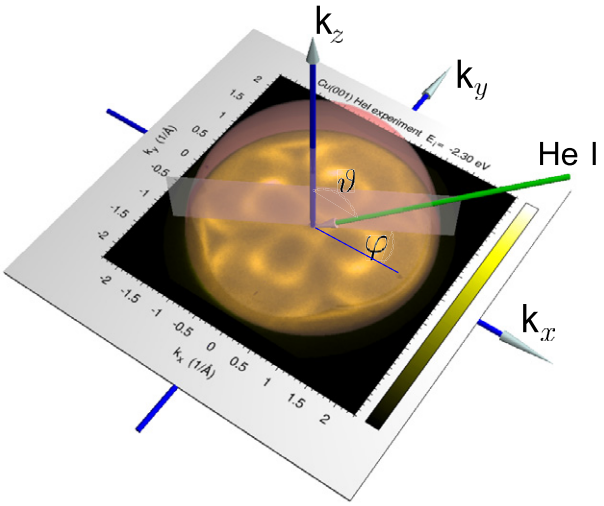

Figure 1. The experimental coordinate system. HeI radiation is incident along the angles $\vartheta = 65^\circ$ and $\varphi = 30^\circ$. The electron-optical axis of the momentum microscope is along the z-direction. The photoelectron intensity is plotted as a function of the in-plane momentum components k_x and k_y for a fixed kinetic energy, with lighter color indicating higher intensity.

(Bohr radii). The electronic structure is analyzed by means of spectral densities

$$N_l(z, \boldsymbol{k}_\parallel) = -\frac{1}{\pi}\mathrm{Im}\,\mathrm{Tr} G_{ll}(z, \boldsymbol{k}_\parallel).$$

Here, z is a complex energy and G_{ll} is the layer-diagonal Green function (l is layer index) at z and the surface-parallel reciprocal vector $\boldsymbol{k}_\parallel = (k_x, k_y)$. By taking partial traces, N_l can be decomposed with respect to orbital momentum, spin projection or irreducible representation of the 'small group' of $\boldsymbol{k}_\parallel$.

The photoemission spectra were computed within the one-step model, using the self-consistent potentials as the input. Photoelectrons were gathered from the topmost 30 layers of the Cu surface. The maximum angular momentum was $l_{\max} = 4$.

Lifetime effects in the photoemission process were emulated by an imaginary part of the energy, that is, the optical potential V_{oi}. For the occupied states, we deliberately choose $V_{\mathrm{oi}} = 0.05\,\mathrm{eV}$. This rather small value allowed us to discriminate the flat d bands in the photoemission spectra. For the unoccupied states, we took $V_{\mathrm{oi}} = 1\,\mathrm{eV}$.

As expected for LDA that has difficulties in describing localized states correctly, the d bands were too high in energy as compared to experiment. Instead of the computationally demanding GW calculations [6], LDA + U or dynamical mean-field calculations, we improved the binding-energy mismatch by a simplified approach, shifting the LDA potentials of Cu by $\Sigma_{\mathrm{d}} = -0.8\,\mathrm{eV}$ for the d states and by $\Sigma_{\mathrm{sp}} = +0.3\,\mathrm{eV}$ for the sp states. These orbital-dependent shifts, which are used to treat the real parts of the self-energy, have been deduced from experiments by Strocov *et al* [35], who were using a band-mapping procedure combining photoemission and very-low-energy electron diffraction. Because our approach acts already on the potentials rather than being a 'scissors operator' on the energy bands, it influences not only energy levels but also wavefunctions. In particular, the shifts of bulk and surface states are different because surface states are subjected to the unmodified vacuum potentials while

bulk states are not. Therefore, this simplified approach leads to improved quantitative agreement between experimental and theoretical dispersion relations for surface and bulk states (see section 4) but, undoubtedly, leaves room for improvement.

The present approach can be regarded as the very first step towards a more complete description of the effects of the electronic self-energy Σ in the photoemission calculations. Being a non-local operator, Σ depends on energy, wavevector $\boldsymbol{k}_{\parallel}$, layer l and orbital momentum. Here, we assumed that Σ is orbital dependent and constant otherwise, which yields satisfactory agreement between experiment and theory. However, given the complete experimental mapping of the valence electronic structure, a detailed comparison of the theoretical momentum patterns with the extensive amount of our energy-dependent 2D experimental momentum data provides a crucial test for advanced calculations of Σ.

4. Results

4.1. Cu(001)

We first address the effects of theoretical self-energy corrections for the d and sp states (Σ_{d} and Σ_{sp}; see section 3) in photoelectron momentum patterns from Cu(001). Therefore, in figure 2(a) we analyze photoemission intensities measured at two different energies: one from the Cu(001) Fermi level ($E_i = 0.00\,\mathrm{eV}$) and the other from the d-band region at an initial energy of $E_{\mathrm{i}} = -2.30\,\mathrm{eV}$. The corresponding theoretical calculations are shown in figure 2(b) neglecting any self-energy-related corrections and in figure 2(c) applying self-energy corrections $\Sigma_{\mathrm{d}} = -0.8\,\mathrm{eV}$, $\Sigma_{\mathrm{sp}} = +0.3\,\mathrm{eV}$ as obtained from [35]. The energy resolution assumed in the calculations was 100meV.

We can already discriminate important effects from the results shown in figure 2. Firstly, the theoretical Fermi-level intensity distribution already fits the experiment quite well when no self-energy shifts are included. Secondly, in contrast to the Fermi level pattern, the calculated photoelectron momentum pattern from the d-band region does not fit the experiment at all when self-energy corrections are neglected. This clearly indicates that different self-energy corrections are necessary for different binding energies and that a rigid shift of the theoretical calculation ('scissors operator') cannot bring the calculation into full agreement with the experiment. This is consistent with the established band-dependent and binding energy-dependent self-energy effects which actually include shifts of *opposite* sign for the Cu d states as compared to the Cu sp states near the Fermi level [35]. As we will show below, another important condition that prohibits a rigid shift of the complete bulk band structure is the necessity to describe the surface electronic structure correctly (see the results for Cu(111) in section 4.2).

As we can see in figure 2(c), the inclusion of self-energy corrections leads to very good agreement both for the Fermi level pattern and for the d-band pattern. A comparison of the actual intensities in figure 2(a) also reveals the clear reproduction of deviations from the fourfold symmetry of the Cu(001) substrate. The (001) surface by itself has fourfold symmetry (point group $4mm$) which, however, is broken in the complete photoemission setup by the off-normally incident light away from an exact mirror plane of the crystal (see the experimental setup in figure 1). As an effect of this symmetry breaking, we see for example that the triangular structure on the bottom left of the d-band pattern in figure 2(c) has higher intensity than its symmetry-correlated sibling on the top right, which is almost suppressed in theory as well as

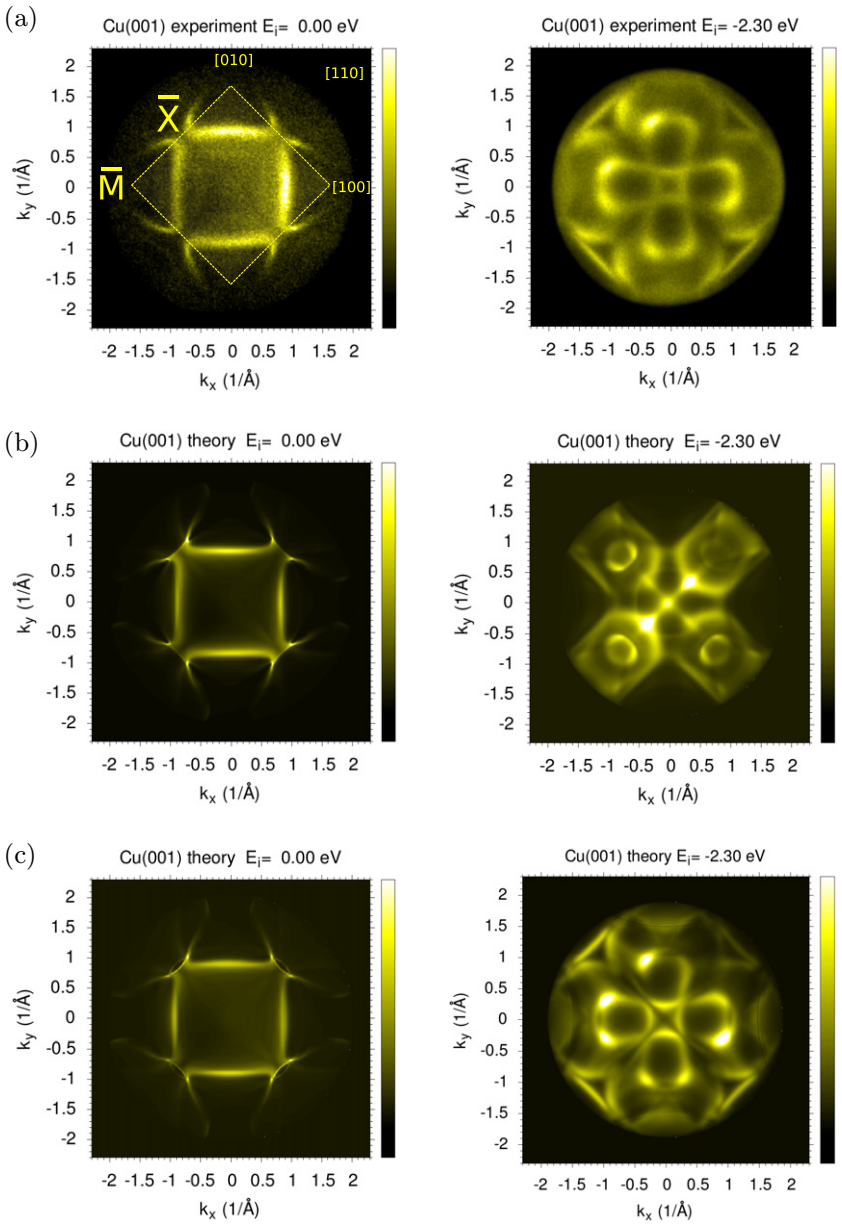

Figure 2. Sensitivity of experimental Cu(001) photoelectron momentum distribution maps to self-energy corrections in one-step photoemission calculations. The surface Brillouin zone is shown on the left in the top row, with the axes of k_x and k_y pointing along the bulk directions [100] and [010], respectively. The patterns are normalized to their respective mean intensities. (a) Cu(001) experiment, Fermi level (left) and $E_\mathrm{i} = -2.3\,\mathrm{eV}$ (right). (b) Theory, no self-energy corrections included. (c) Theory, using $\Sigma_\mathrm{d} = -0.8\,\mathrm{eV}$, $\Sigma_\mathrm{sp} = +0.3\,\mathrm{eV}$.

in experiment. This demonstrates that the symmetry-breaking effects of the incident light are consistently treated in the simulations. The agreement between theory and experiment is of course not perfect. For instance, the nodal lines crossing the surface Brillouin zone center in the

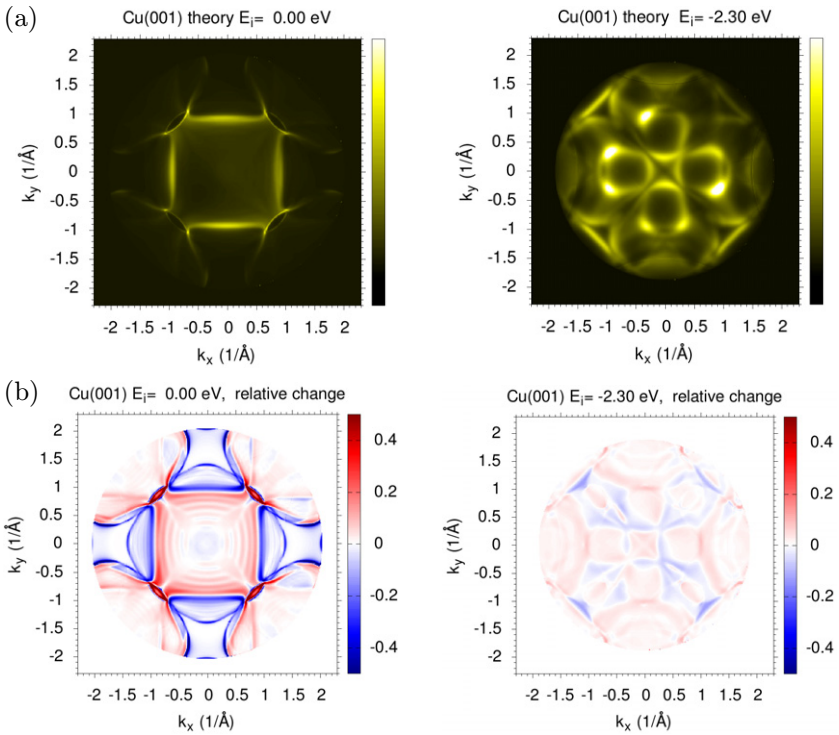

Figure 3. Specific effect of sp-band self-energy corrections on the Cu(001) momentum distribution maps with constant d-state correction $\Sigma_d = -0.8\,\text{eV}$. In the maps of the relative changes A_{sp} as defined in equation (1), red indicates the additional intensity for $\Sigma_{sp} = +0.3\,\text{eV}$ and blue indicates less intensity as compared to $\Sigma_{sp} = 0.0\,\text{eV}$. The sp-state corrections have a weaker relative effect in the d-band region, as is seen in the lower right pattern by the correspondingly reduced modulation. (a) Theory, $\Sigma_d = -0.8\,\text{eV}$, $\Sigma_{sp} = 0.0\,\text{eV}$. (b) Theory, relative change of corrected map for two parameters ($\Sigma_d = -0.8\,\text{eV}$, $\Sigma_{sp} = +0.3\,\text{eV}$) with respect to the $\Sigma_{sp} = 0.0\,\text{eV}$ shown above.

theoretical d-band pattern become filled in experiment. This could be due to the background of inelastically scattered electrons in experiment or by the use of an insufficient lifetime broadening in theory. Nevertheless, we obtain very good overall agreement between experiment and the self-energy corrected theory.

In the calculations shown in figure 2(c), the self-energy correction effects for the d states are much larger than those for the sp states at the Fermi level, which were already quite well described by the uncorrected theory. In order to demonstrate the energy-dependent effects of orbital-dependent self-energy corrections on the momentum patterns, we show in figure 3 the theoretical distributions for the case when we only considered the corrections in $\Sigma_d = -0.8\,\text{eV}$ but neglected the sp-state corrections by setting $\Sigma_{sp} = 0.0\,\text{eV}$. At first sight, the patterns without sp corrections seem to show very similar agreement to the experiment as the previous results in figure 2 containing additional sp-specific corrections $\Sigma_{sp} = +0.3\,\text{eV}$. A closer inspection, however, reveals important differences, which are best recognized when calculating the relative k-resolved intensity change A_{sp} between the theoretical models with and without sp corrections

as

$$A_{\mathrm{sp}} = \frac{I(\Sigma_{\mathrm{sp}} = +0.3\,\mathrm{eV}) - I(\Sigma_{\mathrm{sp}} = 0\,\mathrm{eV})}{I(\Sigma_{\mathrm{sp}} = +0.3\,\mathrm{eV}) + I(\Sigma_{\mathrm{sp}} = 0\,\mathrm{eV})}. \tag{1}$$

The results are seen in the color plots in the lower part of figure 3, where red indicates additional intensity in the pattern with $\Sigma_{\mathrm{sp}} = +0.3\,\mathrm{eV}$ and blue indicates reduced intensity with respect to the pattern with $\Sigma_{\mathrm{sp}} = 0.0\,\mathrm{eV}$. Due to the high density of d states, Σ_{d} shows a dominating influence in the energy range reaching approximately from -4 to $-2\,\mathrm{eV}$. As expected, the relative influence of Σ_{sp} is small in the d-band region, as becomes evident when comparing the magnitudes of the asymmetry patterns for the Fermi level pattern on the left and the $-2.3\,\mathrm{eV}$ pattern on the left. For the d-band pattern the relative change introduced by $\Sigma_{\mathrm{sp}} = +0.3\,\mathrm{eV}$ is moderate with values less than 10%. This observation is fully confirmed by the angular-momentum-resolved band structure, where the contribution of the sp orbitals is small at the d-band energies. In the sp-band region near the Fermi level, however, the sp corrections show a more noticeable effect towards a closing of the intensity gaps near the $\bar{X}$ point, which is seen by the red color near the $\bar{X}$ positions. This trend is in good agreement with the experimental observations (left pattern in figure 2(a)) which show a smaller intensity gap as is produced in the calculations neglecting Σ_{sp} (left pattern in figure 3(a)).

At this point, we can conclude that the introduction of a self-energy correction for the sp bands that is of opposite sign compared to the d states undoubtedly improves the agreement of the calculations with the experimental observations.

Strocov and coworkers [35] deduced slightly energy-dependent values for Σ_{d} and Σ_{sp}. In the present study, we took the mean values of -0.8 and $+0.3\,\mathrm{eV}$. This approximation seems to be justified in view of the resulting agreement between experimental and theoretical momentum distributions in the entire valence-band range.

In our present approach, we cannot include the effects of a band-dependent imaginary part of the self-energy. Instead, the optical potential is used to handle the energy-dependent lifetime-broadening without specific k- or orbital dependence. In addition, this approach only emulates the reduction of the number of elastically scattered electrons and disregards the effects of inelastically scattered photoelectrons that might be present in the experimental energy window. One main effect resulting from inelastic scattering in experiment is the increasing background for lower kinetic energies. Another effect is thermal disorder or other disorders which introduces the possibility for non-direct transitions and thus a loss of k-information from the band structure [43, 44]. While these effects go beyond our current treatment, we point out that we are clearly observing features showing different degrees of sharpness; for instance, compare the sharp and more diffuse features in the top row of figure 4. These characteristically different features are consistently reproduced by the theory, which means that the different sharpness is probably not mainly due to varying k-dependent imaginary parts of the self-energy. Instead, the specific k-space extension of direct optical transitions is mainly related to the degree of dispersion of the relevant initial and final electronic bands [45].

We show additional representative data for four additional energies in figure 4. There, only the kinetic energy of the photoelectrons changes while all other parameters are kept constant in the calculation. The photoelectron distributions vary strongly with initial energy E_{i} and show clearly that both the experimental approach and the calculations capture the intricate details of the flat d bands.

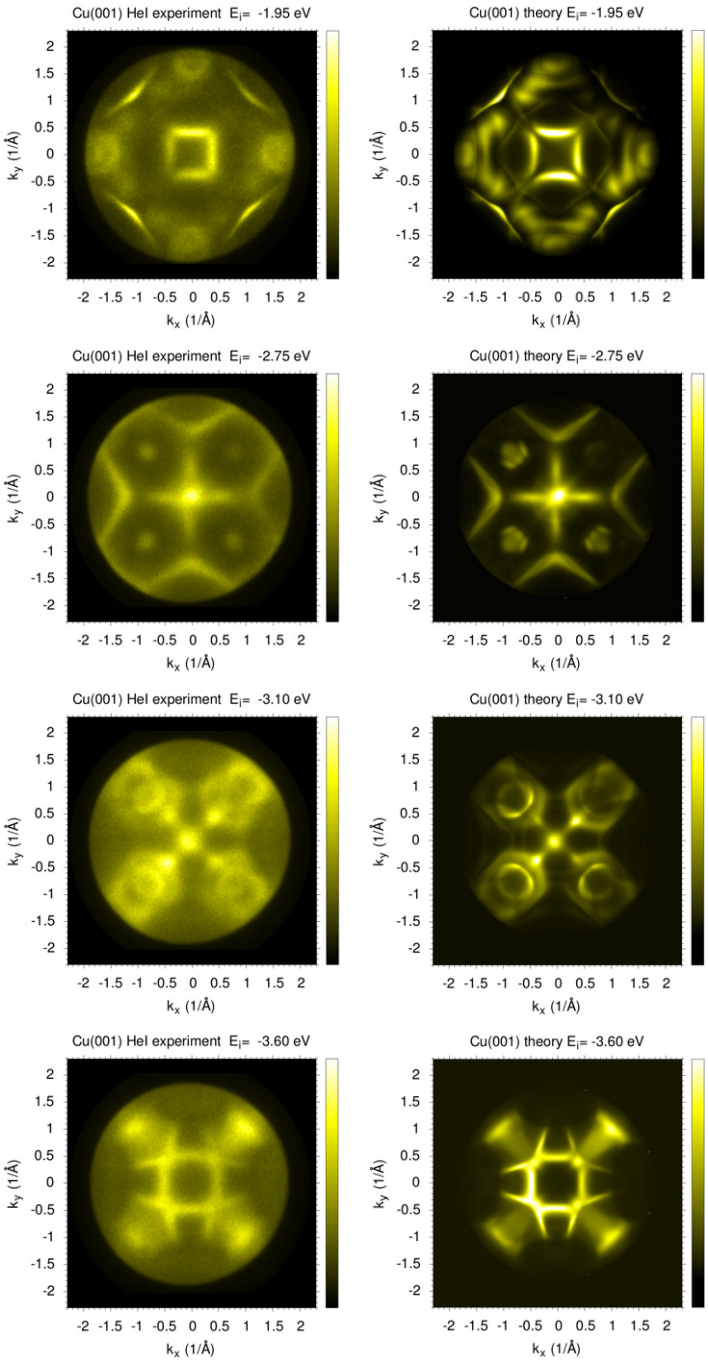

Figure 4. Selected momentum distributions of photoelectrons excited from the Cu(001) d-band region. Experiment on the left and theory on the right; energy levels from the top: $E_i = -1.95$, -2.75, -3.10 and -3.60 eV.

4.2. Cu(111)

After establishing the necessary self-energy corrections for the Cu(001) sample, we applied our approach to measurements at Cu(111) surfaces to test whether the same theoretical parameters give similar agreement to experiments. Moreover, since the Cu(111) surface contains the

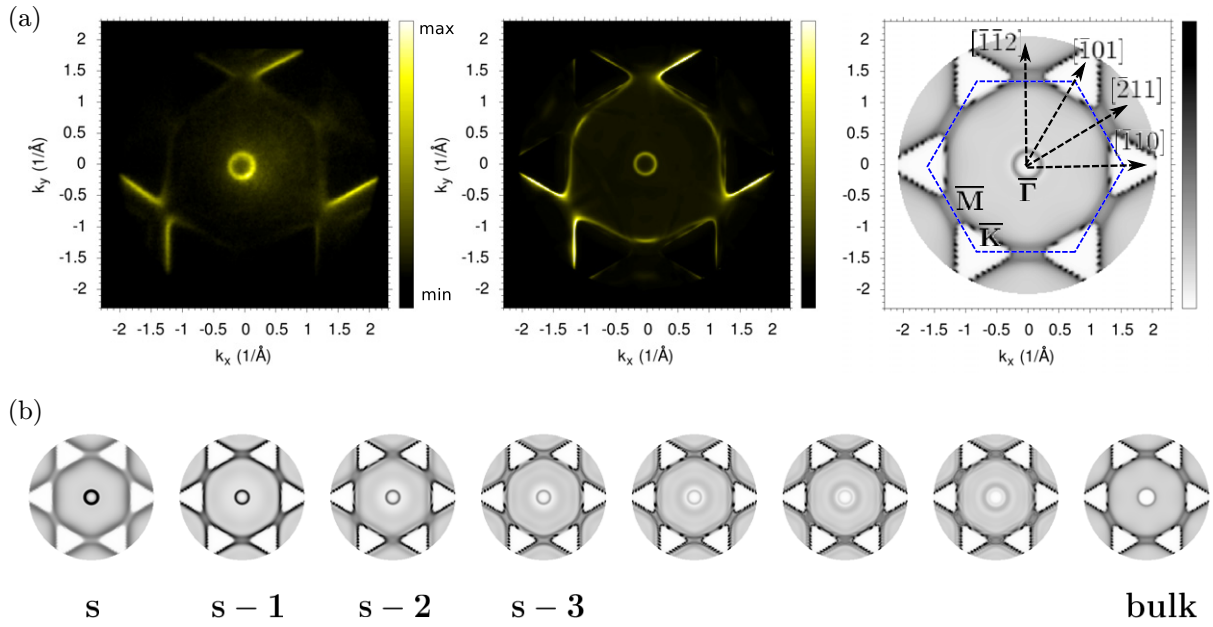

Figure 5. Full-hemispherical photoemission from the Cu(111) Fermi level, $h\nu = 21.2\,\text{eV}$. (a) Left: experiment; middle: theory; right: spectral density with the surface Brillouin zone and major bulk directions. (b) Layer-resolved contributions to the spectral density (the k-region is the same as in part (a) of this figure): left: surface layer(s); right: bulk layer. The Shockley surface state can be seen in the vicinity of $k_{\parallel} = 0$ decaying into the bulk.

prominent L-gap Shockley surface state, we can analyze the implications of the self-energy corrections for the surface electronic structure.

The Cu(111) sample is oriented such that $[\bar{1}10]$ is along the x-axis and $[\bar{1}\bar{1}2]$ along the y-axis (right panel in figure 5(a)). For measurements at the Cu(111) Fermi level, using the same self-energy correction parameters as for Cu(001), we find that the experimental (left panel in figure 5(a)) and theoretical (center) patterns agree very well. For comparison, we show in the right panel of figure 5(a) the relevant surface-projected initial state spectral density of states, which for the Fermi level corresponds to a combination of a 2D projection of the bulk 3D Fermi surface and the 2D surface density of states.

The $\boldsymbol{k}_{\parallel}$-dependent spectral density of states $N_l(E, \boldsymbol{k}_{\parallel})$ in the right panel of figure 5(a) is a sum over the first six surface layers and one bulk layer. Consequently, it consists of contributions from the [111]-projected bulk density of states and an intrinsically surface-localized part which show up in the photoemission intensities. As we can see by making a comparison to the spectral density in the right panel of figure 5(a), the photoemitted signal from the sp bands is not directly proportional to the sixfold symmetric $\boldsymbol{k}_{\parallel}$-projected spectral density. This is due to two main effects. Firstly, apart from the Shockley surface state (discussed below) at small $\boldsymbol{k}_{\parallel}$, we observe bulk transitions which have threefold symmetry around the [111] surface normal. Secondly, a reduction of symmetry is caused by the excitation light, which is incident approximately in the plane spanned by the [111] surface normal and the $[\bar{2}11]$ direction (see figure 1 and the left part of figure 5(a)). Although the light is unpolarized, the transversal character of the

unpolarized light with respect to the incidence direction causes a directional dependence of the transition matrix elements. The sharp, rather line-like photoemission features at large $\boldsymbol{k}_{\parallel}$ in figure 5(a) originate from transitions of the nearly free-electron-like sp bands at the Fermi level. In contrast, the central circular contour is associated with the quasi-2D Shockley surface state, as will become clear in the following.

Our theoretical LKKR approach allows us to distinguish the surface and the bulk contributions by their layer dependence. Figure 5(b) shows a sequence of layer-resolved spectral-density distributions for the Cu(111) Fermi level, starting at the surface (s) towards the bulk. The central circular feature decays rapidly with increasing depth. Furthermore, the bulk distribution (the outermost panel on the right side) is given by the 2D projection of the Cu Fermi surface with the well-known L gap necks along the eight equivalent Γ–L directions. Since no signature of the circular feature is visible anymore in the bulk layer, this feature must indeed be due to a surface state. An orbital-momentum decomposition yields that the Fermi level pattern of figure 5 consists mainly of p-contributions (orbital momentum $l = 1$), as expected for this type of surface states [46].

The Fermi level intensity presented in figure 5 is in principle well known from previous angle-dependent investigations [13], using step-wise measurements of the photoelectron spectrum in a large number of discrete directions with a correspondingly large measurement time. For comparison, the data acquisition of figure 5 took a total of 10 min using the non-monochromatized HeI laboratory light source.

In analogy to the Fermi level photoemission, we recorded the $\boldsymbol{k}_{\parallel}$-resolved photoemission intensities from electronic states in the full accessible valence-band energy region. Examples of the d-band region, reaching from approximately -4 to -2 eV with respect to the Fermi level, are shown in figure 6 (left column), side by side with their calculated counterparts (central column) and the respective spectral densities of the initial states (right column). The overall very good agreement of the Cu(111) momentum distributions seen in figure 6 indicates the transferability of the self-energy corrections to different Cu surfaces.

Compared to the relatively simple structure near the Fermi level caused by sp-like states, the intensity distributions in figure 6 contain a mixture of d, p and s states in the d-band region and are much more complicated. The comparison of the spectral densities of the initial states (right) with the experimental and theoretical intensities illustrates nicely the limited predictive power of the spectral density by itself: the intensity distributions are strongly determined by optical matrix element effects which emphasize certain features and structures in the spectral-density maps.

In order to reveal the influence of the self-energy corrections in the case of Cu(111), we show the energy- and k_y-dependent intensity distributions for Cu(111) in figure 7(a). This corresponds to cuts along $k_x = 0$ of the complete valence-band region measured. The experimental intensity distribution near the Fermi level in the upper part of figure 7 shows the parabolic Shockley surface state band with a binding energy slightly less than -0.4 eV with respect to the Fermi level and a Fermi vector of about 0.2 Å^{-1}. This is in good agreement with the values and trends published in the literature, considering our experimental conditions. For near-ideal high-resolution measurements at 30 K, a binding energy of 0.435 eV and a Fermi vector of $k_F = 0.215$ Å^{-1} were found for the Shockley surface state on Cu(111) [33]. For energies below the Shockley surface state we see a faint intensity resembling the high-intensity d-band about 2 eV below. This is due to the HeIβ satellite ($h\nu = 23.09$ eV) from the

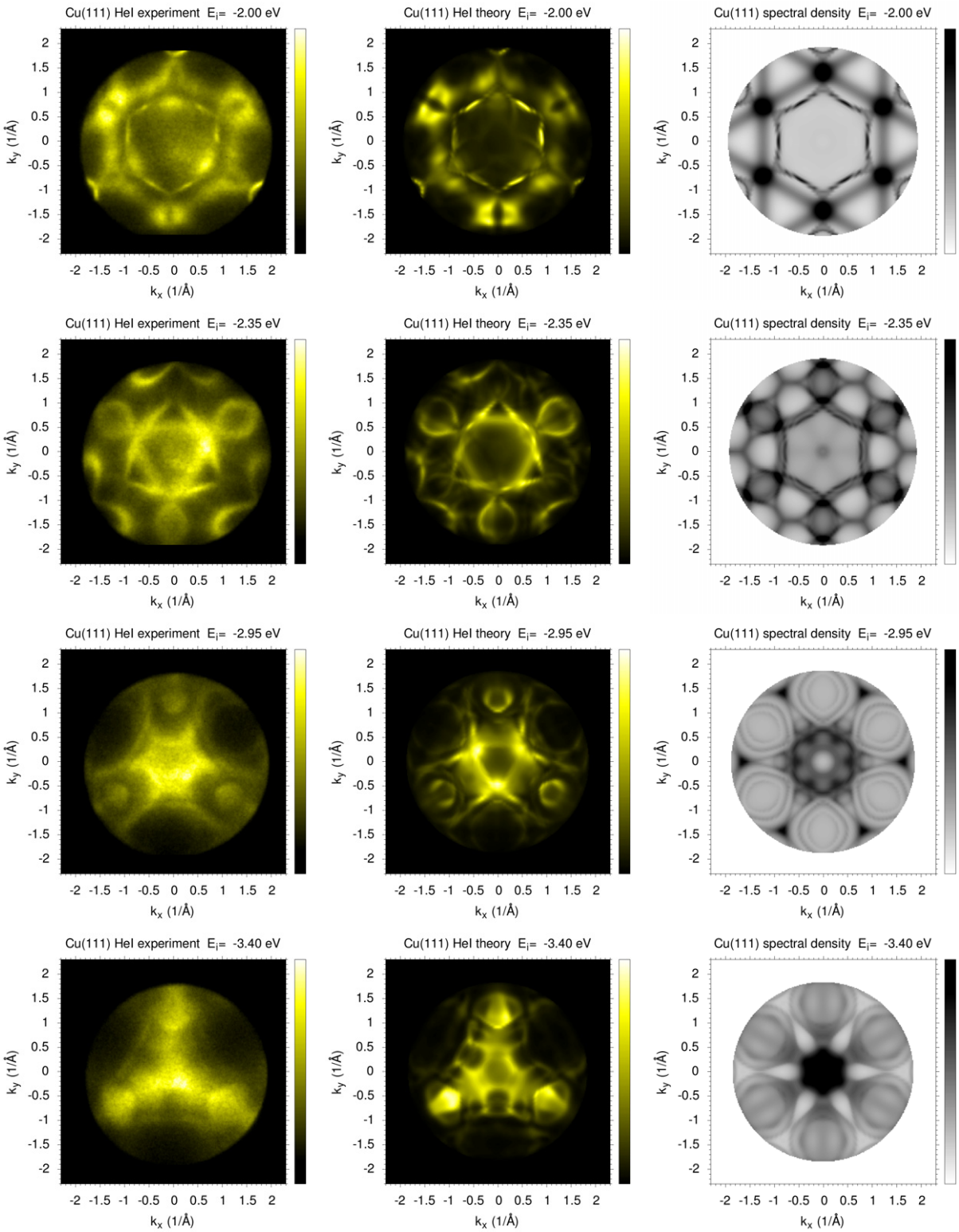

Figure 6. Photoelectron momentum patterns, Cu(111) d bands; left: experiment; middle: theory; right: spectral density of initial states.

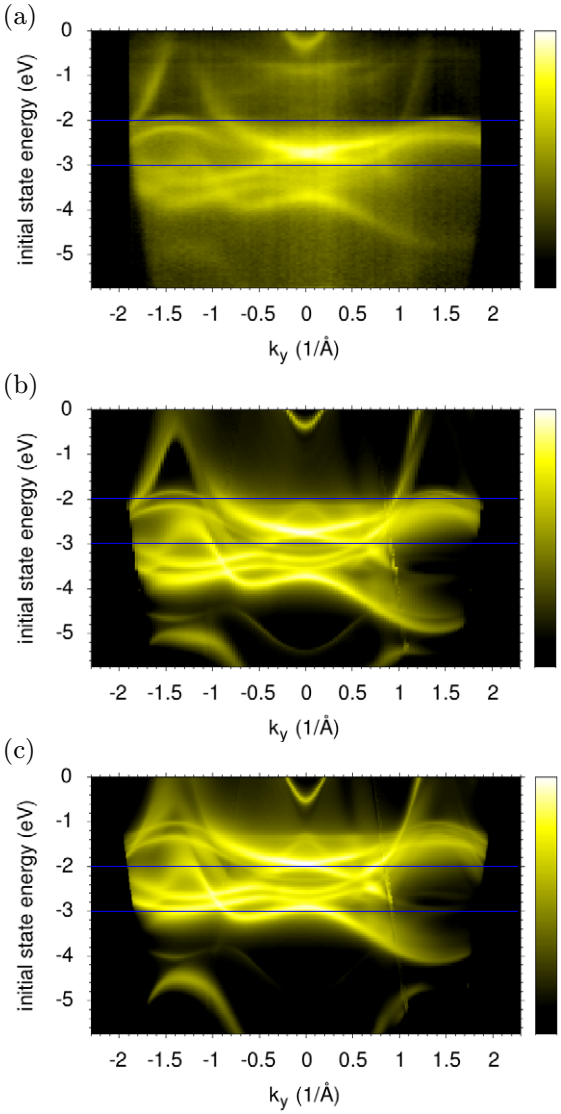

Figure 7. Cu(111), (a) experimental (E, k_y)-intensity plots for $k_x = 0$; (b) comparison to theory assuming self-energy corrections Σ_{sp} and Σ_d; and (c) no self-energy corrections. The horizontal blue lines are for orientation to better judge the energy shifts. (a) Experiment; (b) theory, $\Sigma_d = -0.8\,\text{eV}$, $\Sigma_s = +0.3\,\text{eV}$ self-energy corrections; and (c) theory, $\Sigma_d = 0.0\,\text{eV}$, $\Sigma_s = 0.0\,\text{eV}$ (neglect self-energy corrections).

non-monochromatized He light source. From the measurements, we estimate a contribution of about 2% from HeIβ.

For comparison with the experimental results, the theoretical calculation assuming the self-energy corrections Σ_{sp} and Σ_d is plotted in figure 7(b), again showing good agreement with the experimentally observed features. The additional HeIβ contribution is not included in the theoretical results presented. The influence of the self-energy corrections for the d and sp states is seen from a comparison to the third panel (figure 7(c)), where these corrections

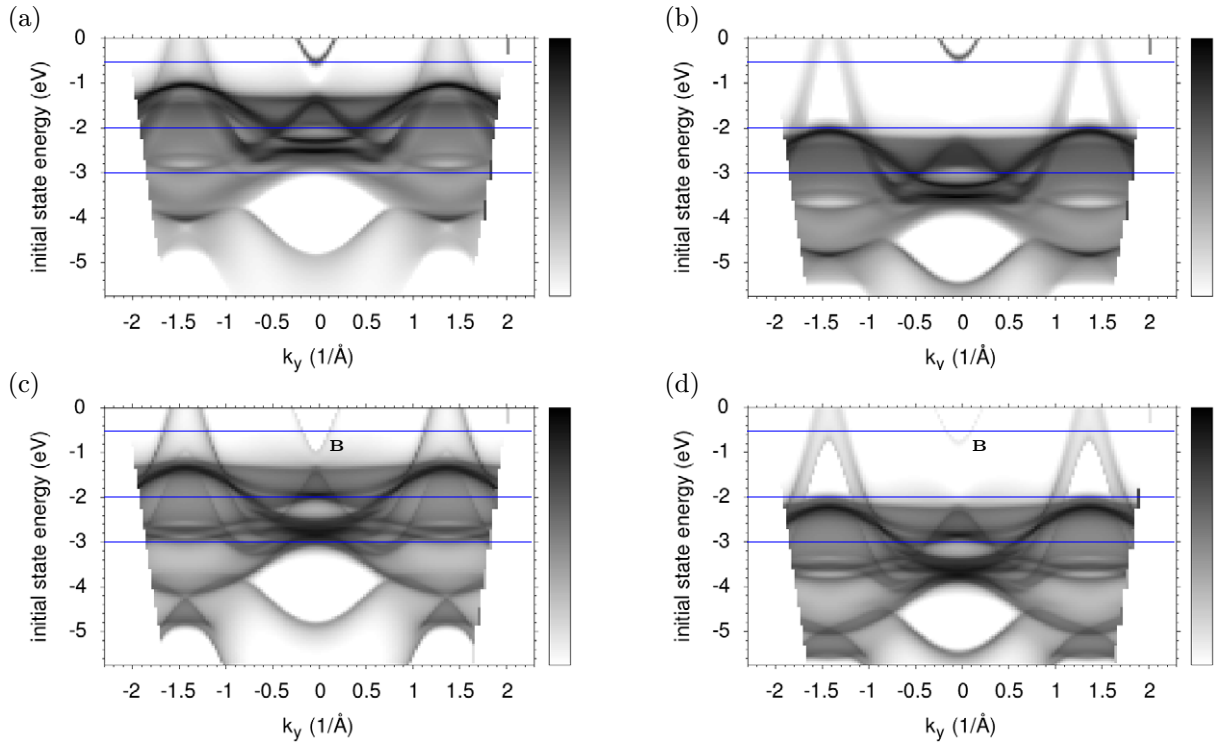

Figure 8. Cu(111), (E, k_y)-spectral density plots for $k_x = 0$ showing the effect of switching on the self-energy corrections (left: no corrections; right: with corrections; the intensity scale is equivalent in all plots; blue lines are guides to the eye). (a) Surface layer, $\Sigma_d = 0.0\,\text{eV}$, $\Sigma_s = 0.0\,\text{eV}$; the uppermost blue line indicates the binding energy of the Shockley surface state seen near $k_y = 0$. (b) Surface layer, $\Sigma_d = -0.8\,\text{eV}$, $\Sigma_s = +0.3\,\text{eV}$. (c) Bulk layer, $\Sigma_d = 0.0\,\text{eV}$, $\Sigma_s = +0.3\,\text{eV}$; the bulk sp-band edge is denoted by 'B', $\Sigma_s = 0.0\,\text{eV}$. (d) Bulk layer, $\Sigma_d = -0.8\,\text{eV}$, $\Sigma_s = +0.3\,\text{eV}$.

have been switched off in the calculation. Among other effects, the result of the downward shift of the d-bands and the upward shift of the sp states is most notably seen by the intensity gap near $k_y = -1.5\,\text{Å}^{-1}$ and at energies from about -0.8 to $-1.8\,\text{eV}$ in both experiment and the calculation including self-energy corrections. In contrast, in the calculation neglecting these corrections, this intensity gap is filled by d states as seen in figure 7(c).

Apart from the bulk-derived features, the self-energy corrections in the calculation influence the surface electronic structure in a specific way. In the surface barrier region, the self-energy corrections can be expected to be reduced when going from the bulk to the vacuum. As noted in the section concerning the theoretical details, we model this in the calculation by neglecting these corrections for the surface barrier.

The overall effect of the bulk self-energy corrections is a reduced binding energy of the Shockley surface state, which is directly visible by the upward shift of the parabolic dispersion when going from figures 7(c) to 7(b). In order to make the surface-related changes more visible, we show in figure 8 the energy-dependent and layer-resolved spectral density of states for the same region as seen in figure 7. The surface layer spectral density is shown in

figures 8(a) and (b), and the bulk layer spectral density in figures 8(c) and (d). As we know from the layer-resolved analysis in figure 5(b), the Shockley surface state is not confined to the uppermost surface layer but penetrates into the bulk considerably. The bulk penetration leads to hybridization effects with the bulk states and a resulting non-parabolic dispersion in the unoccupied states which we have analyzed previously [47]. By the same argument, the self-energy corrections of the bulk should influence the binding energy of the Shockley surface state. In accordance with these expectations, we clearly see from the calculations in figures 8(a) and (b) that the binding energy of the Shockley state changes from $E_B = 0.5\,\text{eV}$ to $E_B < 0.4\,\text{eV}$ with the application of the bulk self-energy corrections. The magnitude of the change is obviously not simply the change in $\Sigma_{sp} = 0.3\,\text{eV}$, as we would expect for the bulk sp bands from which the surface state is derived. Instead, this observation illustrates that the bulk self-energy corrections can have non-trivial effects on the surface states, a fact that in our case leads to improved agreement with the experimental observations. Compared to the established low-temperature values of the binding energy $E_B = 0.435\,\text{eV}$ [33], however, our calculation slightly overestimates the induced shift. Nevertheless, our observations clearly suggest that accounting for bulk and surface-barrier self-energy effects can lead to a better description of angle-resolved photoemission intensities in the presence of bulk and of surface contributions.

The Shockley surface state on Cu(111) is rather stable against slight surface degradations. We emphasize that the experiments reported here were not specially optimized for the observation of other, particularly sensitive surface states which exist on Cu(111) and Cu(001) in several energy regions [48, 49]. A closer look at the experimental and theoretical Cu(001) and Cu(111) data reveals indications of the presence of several such previously reported surface states. In this respect, the momentum microscope is an ideal instrument to analyze surface state effects as we have access to the full surface Brillouin zone in an extended energy range. In future investigations, this should allow us e.g. to distinguish surface states experimentally according to the symmetry and size of the surface Brillouin zone on clean surfaces, adsorbates and overlayers. Because of its inherent depth dependence, our theoretical model is also ideally fitted to an analysis of surface effects in the experiment.

Finally, comparing the conventionally represented, band-structure-like energy- and k_y-dependent data in figures 7 and 8 with the energy-resolved momentum distribution patterns of the other figures, we recognize the complementary information content that is conveyed by the symmetry of (k_x, k_y)-dependent patterns. This should be especially important for photoemission investigations of the orbital components in the electronic states using polarized light.

5. Summary

We have shown that measurements of photoelectron momentum distribution patterns in an extended valence-band energy range can provide essential checks for the effect of many-body corrections in the single-particle band structure of copper. In comparison to the extensive experimental data provided by the momentum microscope, the calculation of photoelectron momentum patterns in the complete accessible valence band represents a *tour de force* in one-step photoemission calculations.

As the energetic positions and wave functions of surface states are closely connected to the underlying bulk band structure, we also demonstrated how the many-body corrections of the bulk also influence the surface electronic structure in a specific way. For the Cu(111) Shockley surface state, we found improved agreement of the calculated binding energy with experiment

if the bulk many-body corrections are included. This points to the importance of many-body corrections for the bulk bands as well as the surface electronic structure.

With the additional option of electron spin-polarization analysis in the momentum microscope [30], the study of spin-dependent many-body effects will be possible.

References

[1] Hüfner S 2003 *Photoelectron Spectroscopy* 3rd edn (Berlin: Springer)

[2] Kevan S D (ed) 1992 *Angle-Resolved Photoemission, Theory and Current Applications* (Amsterdam: Elsevier)

[3] Damascelli A and Shen Z-X 2003 Angle-resolved photoemission studies of the cuprate superconductors *Rev. Mod. Phys.* **75** 473–541

[4] Lee W S, Vishik I M, Lu D H and Shen Z-X 2009 A brief update of angle-resolved photoemission spectroscopy on a correlated electron system *J. Phys.: Condens. Matter* **21** 164217

[5] Schattke W and Van Hove M A (ed) 2003 *Solid-State Photoemission and Related Methods: Theory and Experiment* (Weinheim: Wiley-VCH)

[6] Hedin L 1991 Properties of electron self-energies and their role in electron spectroscopies *Nucl. Instrum. Methods Phys. Res.* A **308** 169–77

[7] Hedin L 1995 Electron correlation: keeping close to an orbital description *Int. J. Quantum Chem.* **56** 445–52

[8] Hüfner S, Claessen R, Reinert F, Straub Th, Strocov V N and Steiner P 1999 Photoemission spectroscopy in metals: band structure— Fermi surface—spectral function *J. Electron Spectrosc. Relat. Phenom.* **100** 191–213

[9] Reinert F and Hüfner S 2005 Photoemission spectroscopy—from early days to recent applications *New J. Phys.* **7** 97

[10] Krüger P, Da Pieve F and Osterwalder J 2011 Real-space multiple scattering method for angle-resolved photoemission and valence-band photoelectron diffraction and its application to Cu(111) *Phys. Rev.* B **83** 115437

[11] Baumberger F, Ingle N, Meevasana W, Shen K, Lu D, Perry R, Mackenzie A, Hussain Z, Singh D and Shen Z-X 2006 Fermi surface and quasiparticle excitations of Sr_2RhO_4 *Phys. Rev. Lett.* **96** 246402

[12] Tamai A *et al* 2008 Fermi surface and van hove singularities in the itinerant metamagnet $Sr_3Ru_2O_7$ *Phys. Rev. Lett.* **101** 026407

[13] Aebi P, Osterwalder J, Fasel R, Naumovic D and Schlapbach L 1994 Fermi surface mapping with photoelectrons at UV energies *Surf. Sci.* **307–309** 917–21

[14] Vobornik I, Fujii J, Hochstrasser M, Krizmancic D, Mulazzi M, Viol C, Panaccione G and Rossi G 2007 k-Space tomography of the Fermi surface by spatially resolved photoemission spectroscopy with variable photon energy *Surf. Sci.* **601** 4246–9

[15] Rader O *et al* 2009 Apparent 'three-dimensional' Fermi surface of transition-metal monolayers *Phys. Rev.* B **79** 245104

[16] Matsui F, Miyata H, Rader O, Hamada Y, Nakamura Y, Nakanishi K, Ogawa K, Namba H and Daimon H 2005 Atomic-orbital analysis of the Cu Fermi surface by two-dimensional photoelectron spectroscopy *Phys. Rev.* B **72** 195417

[17] Tadich A, Riley J, Thomsen L, Cowie B and Gladys M 2011 Determining the orientation of a chiral substrate using full-hemisphere angle-resolved photoelectron spectroscopy *Phys. Rev. Lett.* **107** 175501

[18] Mansson M, Claesson T, Finazzi M, Dallera C, Brookes N B and Tjernberg O 2008 Using high energy angle resolved photoelectron spectroscopy to reveal the charge density in solids *Phys. Rev. Lett.* **101** 226404

[19] Himpsel F J 2011 Angle-resolved photoemission: from reciprocal space to real space *J. Electron Spectrosc. Relat. Phenom.* **183** 114–7

[20] Lee D-W 2010 Method to map one-dimensional electronic wave function by using multiple Brillouin zone angle resolved photoemission *J. Anal. Sci. Technol.* **1** 118–23

[21] Daimon H and Matsui F 2006 Two-dimensional angle-resolved photoelectron spectroscopy using display analyzer. Atomic orbital analysis and characterization of valence band *Prog. Surf. Sci.* **81** 367–86
[22] Takahashi N, Matsui F, Matsuda H, Hamada Y, Nakanishi K, Namba H and Daimon H 2008 Improvement of display-type spherical mirror analyzer for real space mapping of electronic and atomic structures *J. Electron Spectrosc. Relat. Phenom.* **163** 45–50
[23] Dauth M, Körzdörfer T, Kümmel S, Ziroff J, Wiessner M, Schöll A, Reinert F, Arita M and Shimada K 2011 Orbital density reconstruction for molecules *Phys. Rev. Lett.* **107** 193002
[24] Clarke A, Jennings G and Willis R F 1987 Wave-vector imaging photoelectron spectrometer *Rev. Sci. Instrum.* **58** 1439
[25] Coxon P, Krizek J, Humpherson M and Wardell I R M 1990 Escascope—a new imaging photoelectron spectrometer *J. Electron Spectrosc. Relat. Phenom.* **52** 821–36
[26] Tonner B 1995 The development of electron spectromicroscopy *J. Electron Spectrosc. Relat. Phenom.* **75** 309–32
[27] Tonner B P, Dunham D, Droubay T and Pauli M 1997 A photoemission microscope with a hemispherical capacitor energy filter *J. Electron Spectrosc. Relat. Phenom.* **84** 211–29
[28] Tadich A, Riley J, Huwald E, Leckey R, Seyller T and Ley L 2010 Full hemisphere Fermi surface mapping using a novel toroidal electron spectrometer *AIP Conf. Proc.* **1234** 943–6
[29] Krömker B, Escher M, Funnemann D, Hartung D, Engelhard H and Kirschner J 2008 Development of a momentum microscope for time resolved band structure imaging *Rev. Sci. Instrum.* **79** 053702
[30] Tusche C, Ellguth M, Ünal A A, Chiang C-T, Winkelmann A, Krasyuk A, Hahn M, Schönhense G and Kirschner J 2011 Spin resolved photoelectron microscopy using a two-dimensional spin-polarizing electron mirror *Appl. Phys. Lett.* **99** 032505
[31] Courths R 1984 Photoemission experiments on copper *Phys. Rep.* **112** 53–171
[32] Matzdorf R 1998 Investigation of line shapes and line intensities by high-resolution UV-photoemission spectroscopy: some case studies on noble-metal surfaces *Surf. Sci. Rep.* **30** 153–206
[33] Reinert F, Nicolay G, Schmidt S, Ehm D and Hüfner S 2001 Direct measurements of the L-gap surface states on the (111) face of noble metals by photoelectron spectroscopy *Phys. Rev.* B **63** 115415
[34] Strocov V *et al* 2001 Three-dimensional band mapping by angle-dependent very-low-energy electron diffraction and photoemission: methodology and application to Cu *Phys. Rev.* B **63** 205108
[35] Strocov V, Claessen R, Aryasetiawan F, Blaha P and Nilsson P 2002 Band- and k-dependent self-energy effects in the unoccupied and occupied quasiparticle band structure of Cu *Phys. Rev.* B **6** 195104
[36] Baldacchini C, Chiodo L, Allegretti F, Mariani C, Betti M G, Monachesi P and Del Sole R 2003 Cu(100) surface: high-resolution experimental and theoretical band mapping *Phys. Rev.* B **68** 195109
[37] Krutter H 1935 Energy bands in copper *Phys. Rev.* **48** 664–71
[38] Burdick G A 1963 Energy band structure of copper *Phys. Rev.* **129** 138–150
[39] Marini A, Onida G and Del Sole R 2001 Quasiparticle electronic structure of copper in the GW approximation *Phys. Rev. Lett.* **88** 016403
[40] Marini A, Onida G and Del Sole R 2001b Plane-wave DFT-LDA calculation of the electronic structure and absorption spectrum of copper *Phys. Rev.* B **64** 195125
[41] Koller D, Tran F and Blaha P 2011 Merits and limits of the modified Becke–Johnson exchange potential *Phys. Rev.* B **83** 195134
[42] Henk J 2002 Theory of low-energy electron diffraction and photoelectron spectroscopy from ultra-thin films *Handbook of Thin Film Materials, Volume 2: Characterization and Spectroscopy of Thin Films* ed H S Nalwa (San Diego, CA: Academic) chapter 10, pp 479–526
[43] Shevchik N 1977 Disorder effects in angle-resolved photoelectron spectroscopy *Phys. Rev.* B **16** 3428–42
[44] Gray A X *et al* 2011 Probing bulk electronic structure with hard X-ray angle-resolved photoemission *Nature Mater.* **10** 759–64
[45] Strocov V 2003 Intrinsic accuracy in 3-dimensional photoemission band mapping *J. Electron Spectrosc. Relat. Phenom.* **130** 65–78

[46] Bertel E 1994 Symmetry of surface states *Phys. Rev.* B **50** 4925–8
[47] Ünal A A, Tusche C, Ouazi S, Wedekind S, Chiang C-T, Winkelmann A, Sander D, Henk J and Kirschner J 2011 Hybridization between the unoccupied Shockley surface state and bulk electronic states on Cu(111) *Phys. Rev.* B **84** 073107
[48] Yang Y, Wu S, Liu F, Ibrahim K, Qian H, S Lu and Jona F 1996 Surface state at the K point of the surface Brillouin zone on Cu(111) *Phys. Rev.* B **54** 5092–6
[49] Cortona P and Sapet C 2004 The (100), (110), and (111) Cu surfaces revisited by the semiempirical LCAO method *Int. J. Quantum Chem.* **99** 713–23